A Critical Analysis of the Assumptions Underlying the Formulation of Maximum Potential Intensity for Tropical Cyclones

ANASTASSIA M. MAKARIEVA[a,b] AND ANDREI V. NEFIODOV[a]

[a] *Theoretical Physics Division, Petersburg Nuclear Physics Institute, Saint Petersburg, Russia*
[b] *Institute for Advanced Study, Technical University of Munich, Garching, Germany*

(Manuscript received 28 June 2022, in final form 30 January 2023, accepted 8 February 2023)

ABSTRACT: Emanuel's concept of maximum potential intensity (E-PI) estimates the maximum velocity of tropical cyclones from environmental parameters assuming thermal wind (gradient-wind and hydrostatic balances) and slantwise neutrality in the free troposphere. E-PI's key equation relates proportionally the radial gradients of saturated moist entropy and angular momentum. Here the E-PI derivation is reconsidered to show that the thermal wind and slantwise neutrality imply zero radial gradients of saturation entropy and angular momentum at an altitude where, for a given radius, the tangential wind has a maximum. It is further shown that, while E-PI's key equation requires that, at the point of maximum tangential wind, the air temperature must increase toward the storm center, the thermal wind equation dictates the opposite. From the analysis of the equations of motion at the altitude of maximum tangential wind in the free troposphere, it is concluded that here the airflow must be supergradient. This implies that the supergradiency factor (a measure of the gradient-wind imbalance) must change in the free troposphere as the airflow tends to restore the balance. It is shown that such a change modifies the derivative of saturation entropy over angular momentum, which cannot therefore remain constant in the free troposphere as E-PI requires. The implications of these findings for the internal coherence of E-PI, including its boundary layer closure, are discussed.

KEYWORDS: Tropical cyclones; Hurricanes/typhoons; Temperature

1. Introduction

Tropical storms threaten human lives and livelihoods. Numerical models can simulate a wide range of storm intensities under the same environmental conditions (e.g., Tao et al. 2020). Thus, it is desirable to have a reliable theoretical framework that would, from the first principles, confine model outputs to the domain of reality (Emanuel 2020). The theoretical formulation for maximum potential intensity (E-PI) of tropical cyclones by Emanuel (1986) has been long considered as an approximate upper limit on storm intensity [see discussions by Garner (2015), Kieu and Moon (2016), and Kowaleski and Evans (2016)]. Studies have shown that the maximum wind (observed or modeled) can be larger than E-PI due to supergradient wind ("superintensity") (e.g., Persing and Montgomery 2003; Montgomery et al. 2006; Bryan and Rotunno 2009a; Rousseau-Rizzi and Emanuel 2019; Li et al. 2020). Here we reconsider the assumptions behind E-PI to show that they are mutually incompatible at the point of maximum wind.

The E-PI formulation is based on the thermal wind equation and the assumption of slantwise neutrality in the free troposphere. In section 2 we repeat the E-PI derivation following Emanuel (1986) but focusing on the altitude where tangential velocity has a local maximum $\partial v/\partial z = 0$. We show that here E-PI predicts zero radial gradients of saturation entropy s^* and angular momentum thus not permitting nontrivial solutions and being inapplicable for the assessment of maximum winds.

For readers immediately interested in the underlying physics, here is a brief explanation. The gradient-wind balance consists in the equality of the centripetal and centrifugal forces: the radial pressure gradient per unit density and the squared tangential velocity divided by radius. Where $\partial v/\partial z = 0$, the latter force is invariant over z. For the thermal wind equation to apply, the gradient wind (determined by the radial pressure gradient per unit air density) must also be constant over z. In hydrostatic equilibrium, this is the case when the radial and vertical gradients of temperature T over pressure p are equal (see appendix A). When $\partial s^*/\partial z = \partial s^*/\partial r = 0$, this condition is fulfilled: the temperature gradients in both directions are moist adiabatic. In real cyclones, the radial pressure gradient diminishes with height changing its sign in the midtroposphere. The thermal wind equation at the point $\partial v/\partial z = 0$ cannot hold. Another perspective on the same problem is that E-PI constrains the slope of angular momentum surfaces, and this predicted slope is never zero—although it must be so where $\partial v/\partial z = 0$ (see section 6).

In section 3 we discuss why the incompatibility between E-PI's assumptions is not explicit in the resulting E-PI formula. In section 4 we show how this incompatibility can be explicated by combining the E-PI formula with the definition of saturated moist entropy. This reveals that the E-PI formula and the thermal wind equation from which it derives, predict the opposite signs of the radial temperature gradient at the point of maximum tangential wind. In section 5 we discuss additional dynamic constraints on E-PI from the equations of motion. In section 6 we discuss the implications of our findings for the boundary layer closure in E-PI. In view of the

Denotes content that is immediately available upon publication as open access.

Corresponding author: Anastassia M. Makarieva, ammakarieva@gmail.com

DOI: 10.1175/JAS-D-22-0144.1

obtained results, the concluding section 7 discusses the general coherence of E-PI and some issues with its verification by numerical modeling.

2. E-PI derivation for the point where $\partial v/\partial z = 0$

We begin with the consideration of Emanuel's (1986) Eqs. (1)–(8), which describe a steady axisymmetric hurricane vortex. Absolute angular momentum per unit mass is

$$M \equiv vr + \frac{1}{2}fr^2, \tag{1}$$

where v is the tangential velocity and r is the distance from the cyclone center. The Coriolis parameter $f \equiv 2\Omega\sin\phi$ is assumed constant (ϕ is latitude, Ω is the angular velocity of Earth's rotation).

With g as the acceleration of gravity and $\alpha \equiv 1/\rho$ as the specific volume, the hydrostatic balance is

$$\alpha\frac{\partial p}{\partial z} = -g. \tag{2}$$

The radial balance of forces can be written as

$$b\alpha\frac{\partial p}{\partial r} = \frac{v^2}{r} + fv = \frac{M^2}{r^3} - \frac{1}{4}f^2r. \tag{3}$$

Here we have introduced the *supergradiency* factor b. It defines the degree to which the flow is radially unbalanced: $b > 1$ for the supergradient flow when the outward-pushing centrifugal force is larger than the inward-pulling pressure gradient. Emanuel [1986, his Eq. (3)] assumed gradient-wind balance, i.e., $b = 1$.

Using Eq. (2), Eq. (3) can be written as follows:

$$g\left(\frac{\partial z}{\partial r}\right)_p = -g\left(\frac{\partial p}{\partial r}\right)_z\left(\frac{\partial p}{\partial z}\right)_r^{-1} = \frac{1}{b}\left(\frac{M^2}{r^3} - \frac{1}{4}f^2r\right). \tag{4}$$

Hydrostatic equilibrium, (2), is rewritten as

$$g\left(\frac{\partial z}{\partial p}\right)_r = g\left(\frac{\partial p}{\partial z}\right)_r^{-1} = -\alpha. \tag{5}$$

Taking the derivative of Eq. (4) with respect to p at constant r, and of Eq. (5) with respect to r at constant p, we obtain

$$\frac{1}{r^3}\left(\frac{\partial M^2}{\partial p}\right)_r - \left(\frac{M^2}{r^3} - \frac{1}{4}f^2r\right)\frac{1}{b}\left(\frac{\partial b}{\partial p}\right)_r = -b\left(\frac{\partial \alpha}{\partial r}\right)_p. \tag{6}$$

In gradient-wind balance, i.e., with $b = 1$ and $(\partial b/\partial p)_r = 0$, the second term on the left-hand side of Eq. (6) is zero, and it becomes Emanuel's (1986) thermal wind equation.

Emanuel (1986) assumed reversible thermodynamics neglecting the condensate loading.[1] In this case α is a function of p and saturation entropy s^* alone and

$$\left(\frac{\partial \alpha}{\partial r}\right)_p = \left(\frac{\partial \alpha}{\partial s^*}\right)_p\left(\frac{\partial s^*}{\partial r}\right)_p. \tag{7}$$

For the definition of s^* see Eq. (B1) in appendix B.

Using the first law of thermodynamics, it can be shown that $(\partial\alpha/\partial s^*)_p = (\partial T/\partial p)_{s^*} > 0$, where the last expression is the moist adiabatic temperature gradient. Then Eq. (6) becomes

$$\frac{1}{r^3}\left(\frac{\partial M^2}{\partial p}\right)_r - \left(\frac{M^2}{r^3} - \frac{1}{4}f^2r\right)\frac{1}{b}\left(\frac{\partial b}{\partial p}\right)_r = -b\left(\frac{\partial T}{\partial p}\right)_{s^*}\left(\frac{\partial s^*}{\partial r}\right)_p. \tag{8}$$

At this point Emanuel (1986) involved the assumption of slantwise neutrality in the form $s^* = s^*(M)$, i.e., assuming that saturation entropy is a function of angular momentum alone. We will now consider the implications of this assumption applied at the point where $\partial v/\partial z = 0$ together with Eq. (8) where $(\partial b/\partial p)_r = 0$.

Whenever $\partial v/\partial z = 0$, we have $\partial M/\partial z = 0$ and $(\partial M/\partial p)_r = 0$ and, by consequence from Eq. (8), $(\partial s^*/\partial r)_p = 0$. On the other hand, since $s^* = s^*(M)$ and $(\partial s^*/\partial p)_r = (ds^*/dM)(\partial M/\partial p)_r$, we also have $(\partial s^*/\partial p)_r = 0$ (excluding the unrealistic case $ds^*/dM = 0$). But since $(\partial s^*/\partial p)_r = 0$ and $(\partial s^*/\partial r)_p = 0$, this means that whenever $\partial v/\partial z = 0$, the radial gradient of saturation entropy is zero: $\partial s^*/\partial r = 0$. Furthermore, since $\partial s^*/\partial r = (ds^*/dM)\partial M/\partial r$, the radial gradient of angular momentum is also zero: $\partial M/\partial r = 0$. These conclusions do not depend on the value of b.

In real cyclones, saturation entropy increases toward the storm center in the lower atmosphere: $\partial s^*/\partial r < 0$ (e.g., Montgomery et al. 2006, their Fig. 4f). Equation (8) applied for $\partial v/\partial z = 0$ makes it clear that for $\partial s^*/\partial r < 0$ the supergradiency factor b must grow with altitude [i.e., $(\partial b/\partial p)_r < 0$]:

$$\left(\frac{\partial T}{\partial p}\right)_{s^*}\left(\frac{\partial s^*}{\partial r}\right)_p = \left(\frac{M^2}{r^3} - \frac{1}{4}f^2r\right)\frac{1}{b^2}\left(\frac{\partial b}{\partial p}\right)_r. \tag{9}$$

As a side note, the supergradiency factor b can change due to thermodynamics (which controls the pressure gradient) and dynamics (which controls the centrifugal force); see Eq. (3). We show in appendix A that the thermodynamic change of b over z in the boundary layer is small, not exceeding a few percent over 1 km. Any significant deviation from the gradient-wind balance should be due to turbulent friction.

Our conclusion so far is that the thermal wind equation and the assumption of slantwise neutrality are incompatible with $\partial v/\partial z = 0$.

3. E-PI's key relationship

We will now see why this incompatibility is not explicit in the resulting E-PI formula. We put $(\partial b/\partial p)_r = 0$ in Eq. (8). With $b = 1$, the four equations below correspond to Emanuel's (1986) Eqs. (10)–(13).

Using $(\partial s^*/\partial r)_p = (ds^*/dM)(\partial M/\partial r)_p$, Emanuel (1986) divided Eq. (8) by $(\partial M/\partial r)_p$ to obtain

$$\left(\frac{\partial r}{\partial p}\right)_M = \frac{br^3}{2M}\frac{ds^*}{dM}\left(\frac{\partial T}{\partial p}\right)_{s^*}. \tag{10}$$

[1] Makarieva et al. (2023) estimated that the effect of condensate loading on E-PI's formulation is minor.

This equation was integrated along M and $s^* = s^*(M)$ surfaces. The result is

$$\frac{1}{r^2} - \frac{1}{r_o^2} = -\frac{b(T - T_o)}{M}\frac{ds^*}{dM}, \tag{11}$$

where T_o is the temperature at $r = r_o$. The transition from Eq. (8) to Eq. (10) requires $s^* = s^*(M)$ locally. The transition from Eq. (10) to Eq. (11) requires additionally that ds^*/dM is constant over r following M or s^* surface.

For $r_o \gg r$, Eq. (11) takes the form

$$-r^2 b(T - T_o)\frac{ds^*}{dM} = M. \tag{12}$$

Finally, Eq. (12) is multiplied by $\partial M/\partial r$ to yield Emanuel's (1986) Eq. (13), which, with $b = 1$, is E-PI's key equation:

$$-bT\varepsilon\frac{\partial s^*}{\partial r} = \frac{M}{r^2}\frac{\partial M}{\partial r}. \tag{13}$$

Here $\varepsilon \equiv (T–T_o)/T$ can be interpreted as Carnot efficiency; T_o can be a function of b. Makarieva et al. [2023, their Eqs. (35) and (36)] obtained this result, i.e., Eq. (13) with $b \neq 1$, using a different approach. This result can also be obtained from Bryan and Rotunno's (2009a) Eq. (20) using $u = 0$ (see section 5 below and appendix C of Makarieva and Nefiodov 2022). With the gradient-wind assumption relaxed, ε is replaced with $b\varepsilon$, which is greater than Carnot efficiency for supergradient storms.

These derivations, of Bryan and Rotunno (2009a), Makarieva et al. (2023), and Eqs. (10)–(13) with a constant $b \neq 1$, assume that in the free troposphere the air motion conserves not only the angular momentum, but also the supergradiency factor $b \neq 1$. Such motion, while mathematically possible, is not physically plausible: in the real free troposphere the flow will tend to restore the gradient-wind balance, i.e., $b \neq 1$ will change to $b \simeq 1$ (with a minor deviation from unity determined by how small the turbulent friction is). If, as it enters the free troposphere, the airflow is supergradient with $b > 1$, then, as it begins to relax to gradient balance, $(\partial b/\partial p)_r > 0$ in Eq. (8). The absolute magnitude of ds^*/dM retrieved from Eq. (10) is then smaller than it is when $(\partial b/\partial p)_r = 0$. This indicates that $|ds^*/dM|$ should increase in the upper troposphere where the air reaches gradient-wind balance [$b \simeq 1$ and $(\partial b/\partial p)_r \simeq 0$].

Focusing on the point where $\partial v/\partial z = 0$, we notice that E-PI's key equation was obtained by dividing Eq. (8) by $(\partial M/\partial r)_p = 0$, integrating the resulting equation along M surface, and multiplying it again by $\partial M/\partial r = 0$. In the resulting formula, after this dividing and multiplying by zero, the inapplicability of E-PI to the point where $\partial v/\partial z = 0$ became implicit. However, as we show in the next section, it can be explicated at the point of maximum tangential wind.

4. Radial temperature gradient at the point of maximum tangential wind

We will now show that, at the point of maximum tangential wind, where $\partial v/\partial r = \partial v/\partial z = 0$, E-PI's key equation and the thermal wind equation, from which the former is derived, predict the opposite signs for the radial temperature gradient.

a. *Constraints on $\partial T/\partial r$ from the definition of saturation entropy*

Since saturation entropy s^* is a state variable, its radial gradient can be expressed in terms of the radial gradients of air pressure and temperature [see Eq. (B9)]:

$$\frac{T}{1 + \zeta}\frac{\partial s^*}{\partial r} = -\alpha_d \mathcal{C}\frac{\partial p}{\partial r}, \tag{14}$$

$$\mathcal{C} \equiv 1 - \frac{1}{\Gamma}\left(\frac{\partial T}{\partial r}\right)\left(\frac{\partial p}{\partial r}\right)^{-1} = 1 - \frac{1}{\Gamma}\left(\frac{\partial T}{\partial p}\right)_z, \tag{15}$$

where $\zeta \equiv L\gamma_d^*/(RT)$, $R = 8.3$ J mol^{-1} K^{-1} is the universal gas constant, $\gamma_d^* \equiv p_v^*/p_d$, p_v^* is the partial pressure of saturated water vapor, p_d is the partial pressure of dry air, $L \simeq 45$ kJ mol^{-1} is the latent heat of vaporization, Γ (K Pa^{-1}) is the moist adiabatic lapse rate of air temperature [see its definition (B10)], and $\alpha_d \equiv 1/\rho_d$ is the inverse dry air density. Below we assume $\alpha_d \simeq \alpha$, where $\alpha \equiv 1/\rho$ is the inverse air density. Equation (14) does not contain any assumptions but follows directly from the definition of saturation entropy.

Where $\partial v/\partial r = 0$, we have $\partial M/\partial r = v + fr$ and

$$b\alpha\frac{\partial p}{\partial r} = \frac{v}{r}\frac{\partial M}{\partial r} = \frac{M}{r^2}\frac{\partial M}{\partial r}. \tag{16}$$

The last equality assumes $v \gg fr/2$. Combining Eqs. (14)–(16) we obtain an alternative version of Eq. (13):

$$-\frac{bT}{\mathcal{C}(1 + \zeta)}\frac{\partial s^*}{\partial r} = \frac{M}{r^2}\frac{\partial M}{\partial r}, \quad \frac{\partial v}{\partial r} = 0. \tag{17}$$

Equation (13) assumes thermal wind and slantwise neutrality; Eq. (17) assumes $\partial v/\partial r = 0$. Therefore, where $\partial v/\partial r = 0$, Eq. (17) is more general than Eq. (13) and must hold simultaneously with the latter.

Combining Eqs. (13) and (17) and using the definition of $\mathcal{C}$ we obtain

$$\mathcal{C} = \frac{1}{\varepsilon(1 + \zeta)}, \tag{18}$$

$$\frac{\partial p}{\partial r} = \frac{1}{1 - \mathcal{C}}\frac{1}{\Gamma}\frac{\partial T}{\partial r}, \quad \frac{\partial v}{\partial r} = 0. \tag{19}$$

This shows that an E-PI cyclone would only be possible in the presence of a nonzero radial gradient of air temperature at the point of maximum tangential wind.[2] Makarieva et al. (2023) obtained this result for dry E-PI cyclones.

The maximum Carnot efficiency estimated from temperatures T_o and $T = T_b$ observed, respectively, in the outflow

[2] Equations (18) and (19) clarify why hypercanes cannot exist. With $\varepsilon(1 + \zeta) \to 1$, $\mathcal{C} \to 1$ and $\partial T/\partial r \to 0$. The radial pressure gradient in Eq. (19) is then undefined rather than infinite (cf. Emanuel 1988), see also Makarieva and Nefiodov (2022, their appendix B).

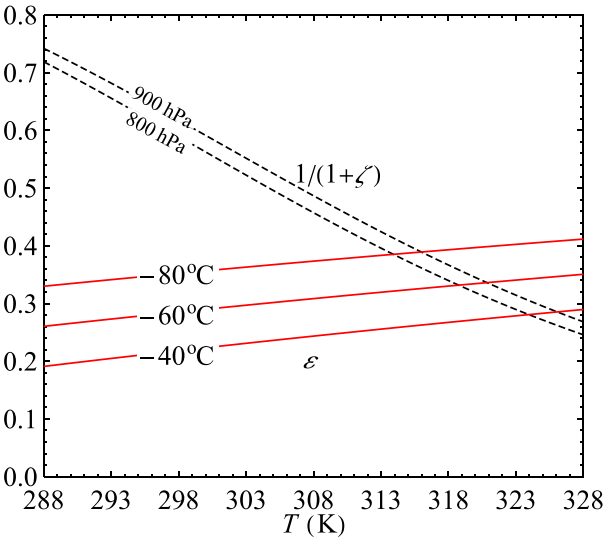

FIG. 1. Parameters $\varepsilon \equiv (T - T_o)/T$ vs $1/(1 + \zeta)$ as dependent on temperature T; ε curves correspond to different outflow temperatures T_o; $1/(1 + \zeta)$ curves correspond to p_d values of 800 and 900 hPa; see Eq. (B10).

and at the top of the boundary layer, is $\varepsilon = 0.35$ (DeMaria and Kaplan 1994). Assuming that T_b does not usually exceed 303 K (30°C), the minimum value of $(1 + \zeta)^{-1} \simeq 0.5$ is larger than ε. It corresponds to the largest $\gamma_d^* \simeq 0.05$ for $T_b = 303$ K and $p_d \simeq 800$ hPa. The partial pressure p_v^* of saturated water vapor and, hence, γ_d^* depend exponentially on air temperature. The realistic temperatures at the top of the boundary layer are commonly significantly lower than 303 K.

Thus, under observed atmospheric conditions $[\varepsilon(1 + \zeta)]^{-1} > 1$ (Fig. 1). This means that for the E-PI cyclone to exist, i.e., for $\partial p/\partial r > 0$, the air temperature must grow in the direction of the cyclone center, i.e., $\partial T/\partial r < 0$ where $\partial v/\partial r = 0$. We emphasize that, to be valid, E-PI requires a specific value of $\partial T/\partial r < 0$ as determined by Eq. (18). At observed temperatures, E-PI requires $\mathcal{C} \simeq 2$ [i.e., $(\partial T/\partial p)_z \simeq -\Gamma$]. Notably, due to the change of the sign of the last term in Eq. (19) at high temperatures, see Fig. 1, E-PI requires that at high temperatures the air temperature at the point of maximum tangential wind should decline in the direction of the storm center, i.e., $\mathcal{C} < 1$.

b. Thermal wind constraints on $\partial T/\partial r$

We will now show that the thermal wind equation does not permit $\partial T/\partial r < 0$ where $\partial v/\partial z = 0$. Hydrostatic balance, (2), can be cast into the following form:

$$\frac{\partial \ln p}{\partial z} = -\frac{1}{h}, \quad h \equiv \frac{RT}{gM_a}, \tag{20}$$

where M_a is air molar mass (here assumed to be constant as in E-PI) and R is the universal gas constant.

Where $\partial v/\partial z = 0$, the derivative with respect to z of the right-hand side of Eq. (3) is zero, so taking into account that $\alpha = gh/p$ according to Eq. (20), we have

$$\frac{\partial b}{\partial z} h \frac{\partial \ln p}{\partial r} + b \frac{\partial h}{\partial z} \frac{\partial \ln p}{\partial r} + bh \frac{\partial}{\partial z}\left(\frac{\partial \ln p}{\partial r}\right) = 0, \quad \frac{\partial v}{\partial z} = 0. \tag{21}$$

Interchanging the order of differentiation in the last term in Eq. (21), using Eq. (20) and noting that $d \ln T = d \ln h$, we obtain

$$\frac{\partial \ln p}{\partial r}\left(\frac{\partial \ln b}{\partial z} + \frac{\partial \ln T}{\partial z}\right) = -\frac{1}{h}\frac{\partial \ln T}{\partial r}, \quad \frac{\partial v}{\partial z} = 0. \tag{22}$$

If the gradient-wind balance holds in the free troposphere, we have $\partial b/\partial z = 0$. Using the definition of h in Eq. (20), Eq. (22) then becomes, cf. Eq. (19),

$$\frac{\partial p}{\partial r} = -\rho g \frac{\partial T}{\partial r}\left(\frac{\partial T}{\partial z}\right)^{-1}, \quad \frac{\partial v}{\partial z} = 0. \tag{23}$$

Since $\partial T/\partial z < 0$, for there to be a cyclone, i.e., for $\partial p/\partial r > 0$, the air temperature must locally decline in the direction of the cyclone center, i.e., $\partial T/\partial r > 0$ where $\partial v/\partial z = 0$.

This result can be directly derived from the thermal wind equation, Eq. (6) of Emanuel (1986) and Eq. (5) of Emanuel and Rotunno (2011); see also our Eq. (6). It says that where the balanced wind is maximum over z, $(\partial M/\partial p)_r = 0$, we have $(\partial \alpha/\partial r)_p = 0$ and, hence, $(\partial T/\partial r)_p = 0$. In the boundary layer of tropical cyclones, the isobars rise outward from the center, $(\partial z/\partial r)_p > 0$. With $\partial T/\partial z < 0$, the coincidence of isobars and isotherms means that $\partial T/\partial r > 0$.

5. Constraints from the equations of motion

For the condition $\partial T/\partial r < 0$ to hold, it follows from Eq. (22) that the supergradiency factor b must increase with altitude at the point of maximum tangential wind, $\partial \ln b/\partial z > -\partial \ln T/\partial z > 0$. We will now show that $b = 1$ is incompatible with $\partial b/\partial z \neq 0$ where $\partial v/\partial z = 0$. It is not possible to retain the gradient-wind balance assumption locally but to relax it in the vicinity of this point.

The steady-state equations of axisymmetric motion for a frictionless atmosphere can be written as

$$\alpha \frac{\partial p}{\partial r} = \frac{v^2}{r} + fv - u\frac{\partial u}{\partial r} - w\frac{\partial u}{\partial z}, \tag{24a}$$

$$0 = \frac{u}{r}\frac{\partial (rv)}{\partial r} + fu + w\frac{\partial v}{\partial z}, \tag{24b}$$

$$\alpha \frac{\partial p}{\partial z} = -g - u\frac{\partial w}{\partial r} - w\frac{\partial w}{\partial z}, \tag{24c}$$

where u is the radial velocity and w is the vertical velocity.

Where $\partial v/\partial z = 0$, the derivative of the right-hand part of Eq. (3) with respect to z is zero, so we have from Eq. (24a)

$$\alpha \frac{\partial p}{\partial r}\frac{\partial \ln b}{\partial z} = -\frac{\partial}{\partial z}\left(\alpha \frac{\partial p}{\partial r}\right) = \frac{\partial u}{\partial z}\frac{\partial u}{\partial r} + u\frac{\partial^2 u}{\partial z \partial r} + \frac{\partial w}{\partial z}\frac{\partial u}{\partial z} + w\frac{\partial^2 u}{\partial z^2}. \tag{25}$$

For $\partial v/\partial z = 0$, we have from Eq. (24b) that $u = 0$. If $b = 1$ in Eq. (3), the sum of the last two terms in Eq. (24a) is zero.

For $u = 0$ and $w \neq 0$ (the eyewall),[3] this means that $\partial u/\partial z = 0$. With $u = 0$ and $\partial u/\partial z = 0$, the first three terms in the right-hand part of Eq. (25) are zero.

The radial velocity u changes its sign at the point of maximum tangential wind, where $u = 0$. Below this point, there is convergence and $u < 0$, while above this point there is divergence and $u > 0$. Usually, the horizontal level that separates $u < 0$ and $u > 0$ is close to the top of the boundary layer; see, e.g., Bryan and Rotunno's (2009a) Fig. 11 for modeling and Montgomery et al.'s (2006) Fig. 4b for real cyclones. From the conditions that $\partial u/\partial z = 0$ at the point where $\partial v/\partial z = 0$ and $\partial u/\partial z \geq 0$ in the vicinity of this point,[4] it follows that the second derivative of u with respect to z is zero at the point where $\partial v/\partial z = 0$. Then the fourth term in the right-hand part of Eq. (25) is zero as well. This means that $\partial b/\partial z = 0$, if $b = 1$ where $\partial v/\partial z = 0$. This shows that it is generally not possible to specify b and $\partial b/\partial z$ independently.[5]

In the eyewall with $\partial u/\partial z > 0$ and $w > 0$, it follows from Eqs. (24a) and (24b) that $b > 1$ for $\partial v/\partial z = 0$. In other words, those tropical cyclones that have their maximum wind in the free troposphere must be supergradient [cf. Eq. (9)]. The conventional *balanced* E-PI, which assumes $b = 1$ in the free troposphere, has no solutions under observed atmospheric conditions. With $b \neq 1$ unknown, E-PI is not a closed theory.

6. Implications for the boundary layer closure in E-PI

We are now in a position to discuss where $\partial v/\partial z = 0$ is realized in real cyclones and in models. Surprisingly, despite all the research emphasis on *maximum potential intensity*, the question of where this maximum is located along the vertical axis does not appear to have received consistent attention: observational studies of vertical v profiles exclude the boundary layer (see below). For case studies, Montgomery et al. (2006, their Fig. 4a) reported that, for Hurricane Isabel (2003), the mean tangential wind in the eyewall ($40 \leq r \leq 50$ km) has a maximum at a height of about 1 km, where it is approximately 50% greater than its surface value of approximately 50 m s^{-1}. Hurricanes Ivan (2004), Wilma (2005), Frances (2004), Helene (2006), and Dennis (2005), as shown, respectively, in Figs. 1c and 7b–d of Stern et al. (2014) and Fig. 5a of Stern and Nolan (2009), display the same feature: for $r \gtrsim 40$ km, the slopes of v contours change sign, thus indicating a maximum of v, at or below 1 km. Peng et al.'s (2018) Figs. 4 and 5 likewise show a maximum of tangential wind at ~0.5 km altitude for their simulated cyclones. Thus, the increase of tangential wind with altitude with a maximum near the top of the boundary layer in the eyewall appears to be a common feature in real storms as well as in models.

In E-PI, Emanuel's (1986) Fig. 1 presents a scheme of the boundary layer with constant s^* surfaces that are vertical and constant M surfaces that are not vertical, but become approximately so at the boundary layer top. This scheme is consistent with the assumption Bryan and Rotunno (2009a, p. 3045) assigned to E-PI, that the maximum gradient wind "is located at the top of the boundary layer" where "viscous terms become negligible." Emanuel and Rotunno (2011, p. 2239) explained that for the boundary layer closure in E-PI it is sufficient that "entropy is well mixed along angular momentum surfaces, which are approximately vertical in the boundary layer," and vertical is how Peng et al. (2018) show these surfaces in their Fig. 10b for E-PI. Smith et al. (2008, p. 553) also interpreted E-PI's boundary layer closure as presuming $\partial v/\partial z = 0$ within the boundary layer. Approximately vertical v contours near the radius of maximum wind can be observed in real storms as well [see, e.g., Stern et al. (2014), their Figs. 1a and 1b for Hurricane Ivan (2004)].

In Bryan and Rotunno's (2009a) control simulation, tangential velocity in the eyewall increases with altitude within the lower 1 km (see their Fig. 4b). According to Bryan and Rotunno (2009a, p. 3050), the assumption that the maximum tangential velocity is achieved at the top of the boundary layer "is needed to match the free-atmosphere component to the boundary layer closure in E-PI." In some discrepancy with this interpretation, Stern and Nolan (2011, their Figs. 5a,c) indicated that E-PI, rather, presumes that the maximum tangential wind is located at the surface $z = 0$, where $\partial v/\partial z < 0$, and monotonously declines with height.[6] Likewise, according to Rousseau-Rizzi and Emanuel (2019), E-PI's maximum tangential wind at the surface exceeds the maximum tangential wind at the boundary layer top. This provides a complementary perspective on the discussed incompatibility between E-PI's assumptions at $\partial v/\partial z = 0$. The thermal wind equation and the assumption of slantwise neutrality constrain the slope of the angular momentum surfaces [see Stern and Nolan 2009, their Eq. (A.14)]. This predicted slope is never vertical (unless $r = 0$), although it must be so where $\partial v/\partial z = 0$.

If the M and s^* surfaces are vertical within the boundary layer, and then on the top of the boundary layer their slope abruptly changes to the one constrained by E-PI's Eq. (12) for the free troposphere, then the radial gradients of M, s^*, T, and p will all have infinite derivatives over z on the top of the boundary layer where this discontinuity occurs. According to

[3] Bryan and Rotunno (2009a, p. 3054) noted that in numerical simulations the point of maximum tangential wind often coincides with the point of maximum vertical wind and that "numerical simulations and observations often show that $u \approx 0$ at the location of maximum tangential velocity."

[4] In mathematical analysis, this point is called *a stationary point of inflection*, or *saddle point*. It is the point on a curve at which the curvature changes sign.

[5] Smith et al. (2008) brought up a related argument. They stated that, with $b = 1$ at the top of boundary layer, E-PI *implicitly* assumed gradient-wind balance within the boundary layer. Emanuel and Rotunno (2011, p. 2239) replied that the boundary layer closure in E-PI did not require such an *explicit* assumption. Smith et al. (2008, p. 553) were correct for their particular model of the boundary layer, which assumed $\partial u/\partial z = \partial v/\partial z = 0$. In this case Eq. (25) yields $\partial b/\partial z = 0$ from $b = 1$.

[6] Stern and Nolan (2011) did not verify this pattern from observations, as they confined their consideration to above 2 km. Subsequent studies retained this limitation (Hazelton and Hart 2013; Stern et al. 2014); the recent study of Fischer et al. (2022) does not show the lower 2 km in their Fig. 8 for the vertical profiles of tangential wind—despite the data being available down to the lowest 500 m.

Emanuel and Rotunno (2011), E-PI's boundary layer closure requires s^* to be well mixed along the approximately vertical M surfaces. The condition $\partial s^*/\partial z = 0$ is generally incompatible with $\partial^2 s^*/(\partial z \partial r) \neq 0$ resulting from the discontinuity on the boundary layer top ($\partial s^*/\partial z$ can be zero only at a certain radius where it must change sign over r). It is therefore pertinent to check to which degree the approximation of verticality is essential for E-PI's boundary layer closure.

E-PI's boundary layer closure constrains $ds^*/dM = (\partial s^*/\partial M)_z$ at the top of the boundary layer as the ratio of the vertical fluxes F_{s^*} and F_M of s^* and M at the sea surface. Originally, Emanuel (1986, p. 593) applied his Eq. (27), valid "for any conservative variable c assumed to be well-mixed in the vertical within a turbulent boundary layer" to angular momentum M, but noted at the same time that M "may not be well mixed in the vertical."[7]

For steady axisymmetric flow, the conservation equation for c reads

$$\frac{1}{r}\frac{\partial(cru)}{\partial r} + \frac{\partial(cw)}{\partial z} = \sigma, \tag{26}$$

where σ is the source/sink, which can also account for diffusion processes [e.g., Bryan and Rotunno 2009b, their Eq. (13)]. Assuming, following Emanuel (1986, p. 593), that within the boundary layer $c = \rho$ is approximately constant, we have

$$\frac{1}{r}\frac{\partial(ru)}{\partial r} + \frac{\partial w}{\partial z} = 0. \tag{27}$$

Taking into account Eq. (27) and neglecting the horizontal diffusion, for $c = M$, Eq. (26) becomes

$$u\frac{\partial M}{\partial r} + w\frac{\partial M}{\partial z} = -\frac{\partial F_M}{\partial z}, \tag{28}$$

where F_M is the vertical flux of M. In Emanuel's (1986) Eq. (27), the second term on the left-hand side of Eq. (28) is absent. The error introduced by omitting the vertical term depends on the ratio w/u. If, near the point of maximum wind, $u \to 0$, while w is at its maximum (Bryan and Rotunno 2009a, p. 3054), the error can be large even if $\partial M/\partial z$ is relatively small compared to $\partial M/\partial r$. On a related note, the absolute angle between the M and s^* surfaces does not provide information about how well $s^* = s^*(M)$ is satisfied in the E-PI context (cf. Tao et al. 2019, their Figs. 3b,d,f).

In the general case of $\partial M/\partial z \neq 0$ and $\partial s^*/\partial z \neq 0$, E-PI's boundary layer closure requires $s^* = s^*(M)$ within the boundary layer. Writing Eq. (26) for $c = s^*$ and using $\partial s^*/\partial r = (ds^*/dM)\partial M/\partial r$ and $\partial s^*/\partial z = (ds^*/dM)\partial M/\partial z$, and Eq. (28), we obtain $ds^*/dM = (\partial F_{s^*}/\partial z)/(\partial F_M/\partial z)$. If ds^*/dM is constant and if both fluxes become zero at the top of the boundary layer, this can be integrated over z to yield $ds^*/dM = F_{s^*}/F_M$. But $s^* = s^*(M)$ within the boundary layer cannot be justified due to turbulence.

Emanuel and Rotunno (2011, p. 2239) referred to the study of Bryan and Rotunno (2009a) as demonstrating that E-PI's boundary closure "is well satisfied in axisymmetric numerical simulations." However, in the control simulation of Bryan and Rotunno (2009a, p. 3049), E-PI's boundary layer closure at the radius of maximum wind is violated by 50%: the diagnosed ratio of surface fluxes is 1.5-fold greater than the diagnosed $(\partial s^*/\partial M)_z$ at the top of the boundary layer, as shown in Bryan and Rotunno's (2009a) Fig. 6. This discrepancy is smaller in their Fig. 7, which presents the simulations of Bryan and Rotunno (2009b). But those simulations were made with a different parameter l_v that controls vertical turbulence effects [l_v = 100 m in the control simulation of Bryan and Rotunno (2009a, their Fig. 6) and l_v = 200 m for simulations of Bryan and Rotunno (2009b) shown in Bryan and Rotunno's (2009a) Fig. 7].

Importantly, according to Bryan and Rotunno (2009b, see their Fig. 2), the value of l_v does not influence the maximum wind speed. At the same time, as the comparison of Bryan and Rotunno's (2009a) Figs. 6 and 7 suggests, parameter l_v is instrumental in bringing E-PI's boundary layer closure in agreement with the simulations. If there exist model parameters that control whether E-PI's boundary layer closure is satisfied, and if such parameters make no impact on the maximum intensity, the inference is that the maximum intensity may not be as profoundly dependent on local surface fluxes as E-PI presumes. This requires further clarifications.

7. Discussion and conclusions

We applied E-PI's assumptions to the altitude of maximum tangential wind ($\partial v/\partial z = 0$), which, according to observations and numerical models, is located near the top of the boundary layer. We showed that here E-PI's assumptions are mutually incompatible and only allow for a trivial solution $\partial s^*/\partial r = 0$ and $\partial M/\partial r = 0$. We also applied E-PI's assumptions to the point of maximum tangential wind ($\partial v/\partial z = \partial v/\partial r = 0$) and showed that here their mutual incompatibility results in contrasting predictions concerning the radial temperature gradient. The thermal wind equation requires it to be positive, while E-PI's key equation constrains it to be negative and dependent on the outflow temperature.

E-PI is based on merging the free troposphere constraints with the boundary layer constraints. The incompatibility of its assumptions pertains to the altitude of maximum tangential wind located on the border between the two atmospheric layers, and has implications for both. We have shown that at the altitude of maximum tangential wind the flow must be supergradient and that its relaxation to the gradient-wind balance in the free troposphere disturbs the constancy of ds^*/dM required by E-PI. In the boundary layer, the verticality of M surfaces assumed in E-PI from the sea surface up to the boundary layer top, is not compatible with the nonverticality of M surfaces required by E-PI in the free troposphere. This disturbs the relationship between ds^*/dM on the boundary layer top and the ratio of the surface fluxes of s^* and M that is required for E-PI's boundary layer closure.

Without addressing these theoretical issues, continued efforts to verify E-PI, or its elements, with numerical simulations may not be conclusive regarding the general validity of

[7] For example, in Bryan and Rotunno's (2009a) control simulation designed to check the E-PI assumptions, M contours near the surface are approximately horizontal (see their Fig. 4).

E-PI. Increasing model complexity without a matching increase in the quality of its independent constraints leads to fuzzier conclusions (Puy et al. 2022). In such a situation, the results of numerical simulations can be misleading. We discuss one example below.

One of our reviewers referred to the study of Tao et al. (2019) as demonstrating an agreement between model simulations and E-PI's Eq. (12), from which Eq. (13) derives. If $(T_b - T_o)$, ds^*/dM and M are known, $v^2 \simeq M^2/r^2$ can be diagnosed from Eq. (12); see Tao et al.'s (2019) Eq. (3):

$$v^2 = -(T_b - T_o)M\frac{ds^*}{dM}. \tag{29}$$

However, while Figs. 5c, 5f, and 5i of Tao et al. (2019) do indeed display a good agreement between predicted and model-derived velocities, they do not validate E-PI's Eq. (12). First, we note that Tao et al. (2019, p. 3007 and p. 2999) recognized that "the model simulated flow can be supergradient within the boundary layer" and thus *defined* the top of the boundary layer as "the altitudes where the maximum tangential winds first agree quantitatively with the maximum gradient winds," i.e., deliberately choosing the altitudes where the gradient-wind balance (approximately) holds. Accordingly, V_t in Tao et al.'s (2019) Figs. 5c, 5f, and 5i is not the actual modeled maximum tangential wind, but "the modeled maximum tangential wind at the boundary layer top" thus defined. Tao et al. (2019, p. 3007) emphasized that in all their simulations the diagnosed maximum v from Eq. (29) (shown by red dots in their Figs. 5c,f,i) was "consistently smaller" than the actual modeled maximum tangential wind (not reported).

From this one could conclude that E-PI's Eq. (12) could be valid if not at the point of maximum tangential wind but at least at a certain altitude where the gradient-wind balance (approximately) holds. But there is an additional caveat. Tao et al. (2019, p. 2999) correctly noted, see Eq. (11) above, that in E-PI ds^*/dM should be constant on M surfaces because of the assumed congruence of s^* and M surfaces. Thus, Tao et al. (2019, p. 2999 and their Fig. 4) diagnosed ds^*/dM *not at the same point* where they diagnosed the tangential wind (at the boundary layer top), but in the outflow region in the upper troposphere. However, their own Figs. 3b, 3d, and 3f make it clear that s^* and M surfaces are not congruent over much of the eyewall (between approximately 2 and 9 km). This means that the values of ds^*/dM in the boundary layer and in the outflow region cannot be assumed equal, as ds^*/dM varies where $s^* \neq s^*(M)$.

While Tao et al. (2019) did not analyze how ds^*/dM varied along the M surfaces, other studies indicate that such variation can be substantial. Figure 5b of Peng et al. (2018) shows simultaneously s^* and M contours and readily allows for the estimation of ds^*/dM in their modeled steady-state vortex. In the boundary layer at the radius $r = 30$ km of maximum wind there are three M contour intervals in one s^* contour interval, while in the outflow region at $r = 80$ km there are only two. This indicates a 1.5-fold increase of the absolute value of ds^*/dM. This increase displays a tendency to continue at larger radii in the outflow [not shown in Peng et al.'s (2018) Fig. 5b]. This is consistent with the decline in $|ds^*/dM|$ for supergradient wind discussed in section 3. If a similar pattern holds for the simulations of Tao et al. (2019), then their use of ds^*/dM from the outflow region would lead to an overestimate of v^2 as diagnosed from Eq. (12) by a factor of 1.5 or more (cf. Peng et al. 2018).

In summary, we are not aware of any studies, either observational or modeling, where the validity of E-PI's Eqs. (12) and (13) would be demonstrated together with the validity of their underlying assumptions. Our alternative Eq. (17) suggests that if a constraint on $\mathcal{C}$ (the degree of adiabaticity of the radial temperature gradient) at the point of maximum wind is found, one could dispense with the consideration of the upper troposphere—as E-PI dispenses with the consideration of boundary layer dynamics when constraining $\mathcal{C}$ from the free troposphere considerations alone [see Eq. (18)]. Considering the boundary layer dynamics, Makarieva and Nefiodov (2022) suggested that $\partial T/\partial r = 0$ and $\mathcal{C} = 1$ at the radius of maximum wind is a plausible assumption, which accuracy could be further investigated.

However, from our perspective, the main, and fundamental, problems of E-PI [and of any other local approach, including the alternative Eq. (17)] pertain to the boundary layer closure. Some were discussed here, but see also Makarieva and Nefiodov (2022). Storm intensity is an integral property of the entire storm's energetics, whereby the energy released over a large area is concentrated in the eyewall to generate maximum wind. It cannot be a local function of the highly variable heat input at the radius of maximum wind (even if one could tune a model to suggest otherwise). We argue for a principally different approach to storm dynamics.

Acknowledgments. The authors are grateful to three reviewers for their useful comments. Work of A. M. Makarieva is partially funded by the Federal Ministry of Education and Research (BMBF) and the Free State of Bavaria under the Excellence Strategy of the Federal Government and the Länder, as well as by the Technical University of Munich–Institute for Advanced Study. The authors thank Václav Vacek, Jan Pokorný, and Milan Vlach for stimulating discussions and support.

Data availability statement. There were no raw data utilized in this study.

APPENDIX A

How Does the Gradient Wind Change over z?

From Eq. (20), we have $\partial p/\partial z = -p/h$, where $h \equiv RT/(gM_a)$, while $\alpha = gh/p$. Using these relations, we have

$$\frac{\partial}{\partial z}\left(\frac{h}{p}\frac{\partial p}{\partial r}\right) = \frac{\partial p}{\partial r}\frac{\partial}{\partial z}\left(\frac{h}{p}\right) - \frac{h}{p}\frac{\partial}{\partial r}\left(\frac{p}{h}\right) = \frac{\partial p}{\partial r}\left(\frac{1}{p}\frac{\partial h}{\partial z} - \frac{h}{p^2}\frac{\partial p}{\partial z}\right)$$
$$- \frac{h}{p}\left(\frac{1}{h}\frac{\partial p}{\partial r} - \frac{p}{h^2}\frac{\partial h}{\partial r}\right) = \frac{1}{p}\frac{\partial p}{\partial r}\frac{\partial h}{\partial z} + \frac{1}{h}\frac{\partial h}{\partial r}$$
$$= \frac{1}{p}\frac{\partial p}{\partial r}\left(\frac{\partial h}{\partial p}\right)_r\frac{\partial p}{\partial z} + \frac{1}{h}\left(\frac{\partial h}{\partial p}\right)_z\frac{\partial p}{\partial r} = (K-1)\frac{1}{h}\left(\frac{\partial h}{\partial p}\right)_r\frac{\partial p}{\partial r}, \tag{A1}$$

where $K \equiv (\partial h/\partial p)_z/(\partial h/\partial p)_r = (\partial T/\partial p)_z/(\partial T/\partial p)_r$. Note that when $(\partial T/\partial p)_r = \Gamma$, then $K = 1 - \mathcal{C}$; see Eq. (15).

The relative change of gradient wind with height is given by

$$\left(\alpha\frac{\partial p}{\partial r}\right)^{-1}\frac{\partial}{\partial z}\left(\alpha\frac{\partial p}{\partial r}\right) = (K-1)\frac{p}{h^2}\left(\frac{\partial h}{\partial p}\right)_r = (1-K)\frac{\partial \ln h}{\partial z}$$
$$= (1-K)\frac{\partial \ln T}{\partial z} = -\frac{\partial \ln b}{\partial z}. \quad \text{(A2)}$$

The last equality in Eq. (A2) follows from Eq. (25) under assumption that $\partial v/\partial z = 0$; it quantifies the change in b due to thermodynamics.

With $\partial v/\partial z = 0$, the supergradiency factor b remains constant over z if the horizontal and vertical gradients of temperature over pressure are equal ($K = 1$). If the atmosphere is horizontally isothermal ($K = 0$), then, with a moist adiabatic lapse rate $-\partial T/\partial z \simeq 5$ K km^{-1}, the relative increase in b will be under 2% over 1 km. If the horizontal temperature lapse rate is minus moist adiabatic ($K \simeq -1$, $\mathcal{C} \simeq 2$), as E-PI approximately requires (see section 4a), then b will increase by no more than 4% over 1 km.

APPENDIX B

Deriving an Alternative for E-PI's Eq. (13)

Moist entropy s per unit mass of dry air is defined as [e.g., Eq. (2) of Emanuel (1988), Eq. (A4) of Pauluis (2011)]

$$s = (c_{pd} + q_t c_l)\ln\frac{T}{T'} - \frac{R}{M_d}\ln\frac{p_d}{p'} + q\frac{L_v}{T} - q\frac{R}{M_v}\ln\mathcal{H}. \quad \text{(B1)}$$

Here, $L_v = L_v(T') + (c_{pv}-c_l)(T-T')$ is the latent heat of vaporization (J kg^{-1}); $q \equiv \rho_v/\rho_d \equiv \mathcal{H}q^*$ is the water vapor mixing ratio; ρ_v is water vapor density; $\mathcal{H}$ is relative humidity; $q^* = \rho_v^*/\rho_d$, $q_l = \rho_l/\rho_d$, and $q_t = q + q_l$ are the mixing ratio for saturated water vapor, liquid water, and total water, respectively; ρ_d, ρ_v^*, and ρ_l are the density of dry air, saturated water vapor, and liquid water, respectively; c_{pd} and c_{pv} are the specific heat capacities of dry air and water vapor at constant pressure; c_l is the specific heat capacity of liquid water; $R = 8.3$ J mol^{-1} K^{-1} is the universal gas constant; M_d and M_v are the molar masses of dry air and water vapor, respectively; p_d is the partial pressure of dry air; T is the temperature; and p' and T' are reference air pressure and temperature.

For saturated moist entropy $s^*(q = q^*, \mathcal{H} = 1)$ we have

$$Tds^* = (c_{pd} + q_t c_l)dT - \frac{RT}{M_d}\frac{dp_d}{p_d} + L_v dq^* + q^* dL_v - q^* L_v\frac{dT}{T}$$
$$= \left(c_p - \frac{q^* L_v}{T}\right)dT - \frac{RT}{M_d}\frac{dp_d}{p_d} + L_v dq^*, \quad \text{(B2)}$$

where $c_p \equiv c_{pd} + q^* c_{pv} + q_l c_l$ and $dL_v = (c_{pv} - c_l)dT$. Equation (B2) additionally assumes $q_t = \text{const}$ (reversible adiabat).

The ideal gas law for the partial pressure p_v of water vapor is

$$p_v = N_v RT, \quad N_v = \frac{\rho_v}{M_v}, \quad \text{(B3)}$$

where M_v and ρ_v are the molar mass and density of water vapor. Using Eq. (B3) with $p_v = p_v^*$ in the definition of q^*,

$$q^* \equiv \frac{\rho_v^*}{\rho_d} = \frac{M_v p_v^*}{M_d p_d} \equiv \frac{M_v}{M_d}\gamma_d^*, \quad \gamma_d^* \equiv \frac{p_v^*}{p_d}, \quad \text{(B4)}$$

and applying the Clausius–Clapeyron law

$$\frac{dp_v^*}{p_v^*} = \frac{L}{RT}\frac{dT}{T}, \quad L \equiv L_v M_v, \quad \text{(B5)}$$

we obtain for the last term in Eq. (B2):

$$L_v dq^* = L_v\frac{M_v}{M_d}\left(\frac{dp_v^*}{p_d} - \frac{p_v^*}{p_d}\frac{dp_d}{p_d}\right) = L_v\frac{M_v}{M_d}\left(\frac{p_v^*}{p_d}\frac{dp_v^*}{p_v^*} - \frac{p_v^*}{p_d}\frac{dp_d}{p_d}\right)$$
$$= L_v q^*\left(\frac{L}{RT}\frac{dT}{T} - \frac{dp_d}{p_d}\right). \quad \text{(B6)}$$

Using the Clausius–Clapeyron law (B5), the ideal gas law $p_d = N_d RT$, where $N_d = \rho_d/M_d$, and noting that $p = p_v^* + p_d$, we obtain for the last but one term in Eq. (B2):

$$\frac{RT}{M_d}\frac{dp_d}{p_d} = \frac{RT}{M_d}\left(\frac{dp}{p_d} - \frac{dp_v^*}{p_d}\right) = \frac{dp}{M_d N_d} - \frac{RTp_v^*}{M_d p_d}\frac{dp_v^*}{p_v^*}$$
$$= \frac{dp}{\rho_d} - L_v\frac{M_v p_v^*}{M_d p_d}\frac{dT}{T} = \frac{dp}{\rho_d} - q^* L_v\frac{dT}{T}. \quad \text{(B7)}$$

Taking into account Eq. (B7), Eq. (B2) reads

$$Tds^* = c_p dT - \alpha_d dp + L_v dq^*. \quad \text{(B8)}$$

Putting Eq. (B6) into Eq. (B8) yields

$$Tds^* = \left[c_p + \frac{L_v q^*}{T}\frac{L(1+\gamma_d^*)}{RT}\right]dT - \left(1 + \frac{L\gamma_d^*}{RT}\right)\frac{dp}{\rho_d}$$
$$= -(1+\zeta)\alpha_d\left(1 - \frac{1}{\Gamma}\frac{dT}{dp}\right)dp. \quad \text{(B9)}$$

Here

$$\Gamma \equiv \frac{\alpha_d}{c_p}\frac{1+\zeta}{1+\mu\zeta(\xi+\zeta)}, \quad \xi \equiv \frac{L}{RT}, \quad \zeta \equiv \xi\gamma_d^* \equiv \frac{L}{RT}\frac{p_v^*}{p_d} \equiv \frac{L_v q^*}{\alpha_d p_d},$$
$$\mu \equiv \frac{R}{C_p} = \frac{2}{7}, \quad \text{(B10)}$$

where $\alpha_d \equiv 1/\rho_d$ is the volume per unit mass of dry air and $C_p \simeq c_p M_d$ is the molar heat capacity of air at constant pressure.

REFERENCES

Bryan, G. H., and R. Rotunno, 2009a: Evaluation of an analytical model for the maximum intensity of tropical cyclones. *J. Atmos. Sci.*, **66**, 3042–3060, https://doi.org/10.1175/2009JAS3038.1.

——, and ——, 2009b: The maximum intensity of tropical cyclones in axisymmetric numerical model simulations. *Mon. Wea. Rev.*, **137**, 1770–1789, https://doi.org/10.1175/2008MWR2709.1.

DeMaria, M., and J. Kaplan, 1994: Sea surface temperature and the maximum intensity of Atlantic tropical cyclones. *J. Climate*, **7**, 1324–1334, https://doi.org/10.1175/1520-0442(1994)007<1324:SSTATM>2.0.CO;2.

Emanuel, K. A., 1986: An air–sea interaction theory for tropical cyclones. Part I: Steady-state maintenance. *J. Atmos. Sci.*, **43**, 585–605, https://doi.org/10.1175/1520-0469(1986)043<0585:AASITF>2.0.CO;2.

——, 1988: The maximum intensity of hurricanes. *J. Atmos. Sci.*, **45**, 1143–1155, https://doi.org/10.1175/1520-0469(1988)045<1143:TMIOH>2.0.CO;2.

——, 2020: The relevance of theory for contemporary research in atmospheres, oceans, and climate. *AGU Adv.*, **1**, e2019AV000129, https://doi.org/10.1029/2019AV000129.

——, and R. Rotunno, 2011: Self-stratification of tropical cyclone outflow. Part I: Implications for storm structure. *J. Atmos. Sci.*, **68**, 2236–2249, https://doi.org/10.1175/JAS-D-10-05024.1.

Fischer, M. S., P. D. Reasor, R. F. Rogers, and J. F. Gamache, 2022: An analysis of tropical cyclone vortex and convective characteristics in relation to storm intensity using a novel airborne Doppler radar database. *Mon. Wea. Rev.*, **150**, 2255–2278, https://doi.org/10.1175/MWR-D-21-0223.1.

Garner, S., 2015: The relationship between hurricane potential intensity and CAPE. *J. Atmos. Sci.*, **72**, 141–163, https://doi.org/10.1175/JAS-D-14-0008.1.

Hazelton, A. T., and R. E. Hart, 2013: Hurricane eyewall slope as determined from airborne radar reflectivity data: Composites and case studies. *Wea. Forecasting*, **28**, 368–386, https://doi.org/10.1175/WAF-D-12-00037.1.

Kieu, C. Q., and Z. Moon, 2016: Hurricane intensity predictability. *Bull. Amer. Meteor. Soc.*, **97**, 1847–1857, https://doi.org/10.1175/BAMS-D-15-00168.1.

Kowaleski, A. M., and J. L. Evans, 2016: A reformulation of tropical cyclone potential intensity theory incorporating energy production along a radial trajectory. *Mon. Wea. Rev.*, **144**, 3569–3578, https://doi.org/10.1175/MWR-D-15-0383.1.

Li, Y., Y. Wang, Y. Lin, and R. Fei, 2020: Dependence of superintensity of tropical cyclones on SST in axisymmetric numerical simulations. *Mon. Wea. Rev.*, **148**, 4767–4781, https://doi.org/10.1175/MWR-D-20-0141.1.

Makarieva, A. M., and A. V. Nefiodov, 2022: Alternative expression for the maximum potential intensity of tropical cyclones. arXiv, 2101.06500v4, https://doi.org/10.48550/arXiv.2101.06500.

——, and Coauthors, 2023: Water lifting and outflow gain of kinetic energy in tropical cyclones. *J. Atmos. Sci.*, https://doi.org/10.1175/JAS-D-21-0172.1, in press.

Montgomery, M. T., M. M. Bell, S. D. Aberson, and M. L. Black, 2006: Hurricane Isabel (2003): New insights into the physics of intense storms. Part I: Mean vortex structure and maximum intensity estimates. *Bull. Amer. Meteor. Soc.*, **87**, 1335–1348, https://doi.org/10.1175/BAMS-87-10-1335.

Pauluis, O., 2011: Water vapor and mechanical work: A comparison of Carnot and steam cycles. *J. Atmos. Sci.*, **68**, 91–102, https://doi.org/10.1175/2010JAS3530.1.

Peng, K., R. Rotunno, and G. H. Bryan, 2018: Evaluation of a time-dependent model for the intensification of tropical cyclones. *J. Atmos. Sci.*, **75**, 2125–2138, https://doi.org/10.1175/JAS-D-17-0382.1.

Persing, J., and M. T. Montgomery, 2003: Hurricane superintensity. *J. Atmos. Sci.*, **60**, 2349–2371, https://doi.org/10.1175/1520-0469(2003)060<2349:HS>2.0.CO;2.

Puy, A., P. Beneventano, S. A. Levin, S. L. Piano, T. Portaluri, and A. Saltelli, 2022: Models with higher effective dimensions tend to produce more uncertain estimates. *Sci. Adv.*, **8**, eabn9450, https://doi.org/10.1126/sciadv.abn9450.

Rousseau-Rizzi, R., and K. Emanuel, 2019: An evaluation of hurricane superintensity in axisymmetric numerical models. *J. Atmos. Sci.*, **76**, 1697–1708, https://doi.org/10.1175/JAS-D-18-0238.1.

Smith, R. K., M. T. Montgomery, and S. Vogl, 2008: A critique of Emanuel's hurricane model and potential intensity theory. *Quart. J. Roy. Meteor. Soc.*, **134**, 551–561, https://doi.org/10.1002/qj.241.

Stern, D. P., and D. S. Nolan, 2009: Reexamining the vertical structure of tangential winds in tropical cyclones: Observations and theory. *J. Atmos. Sci.*, **66**, 3579–3600, https://doi.org/10.1175/2009JAS2916.1.

——, and ——, 2011: On the vertical decay rate of the maximum tangential winds in tropical cyclones. *J. Atmos. Sci.*, **68**, 2073–2094, https://doi.org/10.1175/2011JAS3682.1.

——, J. R. Brisbois, and D. S. Nolan, 2014: An expanded dataset of hurricane eyewall sizes and slopes. *J. Atmos. Sci.*, **71**, 2747–2762, https://doi.org/10.1175/JAS-D-13-0302.1.

Tao, D., K. Emanuel, F. Zhang, R. Rotunno, M. M. Bell, and R. G. Nystrom, 2019: Evaluation of the assumptions in the steady-state tropical cyclone self-stratified outflow using three-dimensional convection-allowing simulations. *J. Atmos. Sci.*, **76**, 2995–3009, https://doi.org/10.1175/JAS-D-19-0033.1.

——, M. Bell, R. Rotunno, and P. J. van Leeuwen, 2020: Why do the maximum intensities in modeled tropical cyclones vary under the same environmental conditions? *Geophys. Res. Lett.*, **47**, e2019GL085980, https://doi.org/10.1029/2019GL085980.